Electron density dependence of the electronic structure of InN epitaxial layers grown on sapphire (0001)

T. Inushima*
Department of Electronics, Tokai University, Kitakaname, Hiratsuka 259-1292, Japan

M. Higashiwaki and T. Matsui
National Institute of Information and Communications Technology, Nukui-Kita, Koganei 184-8795, Japan

T. Takenobu and M. Motokawa
Institute for Materials Research, Tohoku University, Katahira, Sendai 980-8577, Japan
(Received 25 October 2004; revised manuscript received 22 February 2005; published 10 August 2005)

The temperature dependence of the resistivity of InN was investigated as a function of carrier density. The carrier density was changed from $n_e = 1.8 \times 10^{18}$ cm^{-3} to 1.5×10^{19} cm^{-3} by Si doping. The InN investigated showed metallic conduction above 20 K. At lower temperatures there was a resistivity anomaly originating from carrier localization in the *a-b* plane, which was confirmed by the magnetoresistance at 0.5 K. The Shubnikov–de Haas oscillation showed that InN had a spherical Fermi surface and its radius increased according to the increase of n_e when $n_e < 5 \times 10^{18}$ cm^{-3}. In addition, an oscillation corresponding to the constant carrier density of 4.5×10^{12} cm^{-2} was observed in the field applied perpendicular to the *a-b* plane. This oscillation showed an anomalous angle dependence on the magnetic field. Taking into account this density, we determined the critical carrier density of the Mott transition to be 2×10^{17} cm^{-3}. Anisotropy of localization was observed within the *a-b* plane, which indicates that the distribution of the electrons was not uniform in the *a-b* plane. The n_e dependence of the magnetoresistance revealed an electronic structure change around 5×10^{18} cm^{-3}. From these results, an electronic structure at the fundamental absorption edge of InN grown on sapphire (0001) was presented.

DOI: 10.1103/PhysRevB.72.085210 PACS number(s): 73.61.Ey, 72.15.Gd, 74.40.+k

I. INTRODUCTION

Among the group III–nitride semiconductors, InN is a key material for optical and high-temperature device applications.[1] Since it was reported that InN, when it has a band-gap energy less than 1.9 eV, shows unusual physical properties, such as type II superconductivity below 3 K (Ref. 2) and anisotropic critical field,[3,4] many reports concerning the band parameters have been published. Most of these regarded the band-gap energy of InN as being around 0.64 eV because of the coincidence between the photoluminescence peak and the energy position where the square of the absorption coefficient against the photon energy is zero.[5–8] The obtained band-gap energy seems to be in good agreement with that obtained by theoretical calculation, where *d* electrons are taken into account to obtain the band-gap energy of 0.85 eV.[9]

The phonon structure of InN is clear and its six optical phonons have been observed by Raman spectra measurements.[10,11] Their energies are in good agreement with those obtained by *ab initio* calculation,[12] where the *d*-electron contribution has to be taken into account for stabilizing the crystal structure; that is, the 4*d*-semicore electrons of In extend further outside the core and overlap largely with the valence states.

In contrast to the optical properties, electrical properties of InN remain unclear. For example, InN has a high carrier mobility of more than 2000 cm^2 V^{-1} s^{-1} at the carrier density of 3×10^{17} cm^{-3},[13] where it is still in a degenerate condition.

To make clear the electrical properties of InN, one of the most powerful methods is to observe the Fermi surface of InN at low temperatures by the use of magnetoresistance. In a preliminary report, we investigated the electronic structure of degenerate InN by Shubnikov–de Haas (SdH) measurements.[14] The result was, however, very strange. That is, the SdH oscillation depended on the angle between the crystal *c* axis and the applied field and had two components: one originated from the spherical Fermi surface, the other from the anisotropic structure spread in the *a-b* plane. Moreover, negative magnetoresistance was observed in the weak-field region, which indicates that the carrier density investigated was close to the critical carrier density of the Mott transition.

In this paper, we present the temperature dependence of the resistivity, magnetoresistance, and Shubnikov–de Haas oscillation of InN as a function of carrier density in the metallic phase above the Mott transition. The carrier density is controlled by Si doping from 1.8×10^{18} to 1.5×10^{19} cm^{-3}. From the experiments we estimate the critical carrier density of the Mott transition of InN. On the basis of these results, we discuss the electronic structure of InN at the fundamental absorption edge, and propose the most plausible energy band structure of InN. Finally, the problems raised by many reports concerning the band-gap energy, electron accumulation on the surface, and absorption tail anomaly are discussed taking into account the proposed band structure.

TABLE I. Sample conditions used in the experiments. Carrier density n_e is given in 10^{18} cm^{-3}, mobility μ_e is given in 1000 cm^2 V^{-1} s^{-1}. These values are obtained by Hall measurements at room temperature. Samples are listed from left to right in order of Si-doping concentration. Sample no. 252 is the nondoped InN.

Sample no.	252	233	235	236	237	238	245	246	249	247	250	248
n_e	1.8	2.0	2.0	2.2	2.5	3.0	3.7	4.7	7.0	7.6	11	15
μ_e	1.28	1.46	1.39	1.52	1.57	1.60	1.49	1.50	1.34	1.28	1.02	1.00

II. EXPERIMENTAL PROCEDURES

The samples were grown on sapphire (0001) by plasma-assisted molecular-beam epitaxy (MBE). Nitrogen radicals were supplied by an rf plasma cell. The MBE growth started with thermal cleaning and nitridation of the sapphire substrate at 850 °C for 30 min. 10-nm-thick low-temperature GaN and 10-nm-thick low temperature InN layers were grown at 380 °C sequentially. After that, a 250-nm-thick InN layer was grown at 480 °C.[15] Si doping was done in order to change the carrier density. The doping concentration was controlled by the evaporation temperature of the Si-effusion cell from 1120 to 1340 °C. The obtained InN had a carrier density (n_e) from 1.8×10^{18} to 1.5×10^{19} cm^{-3} and a mobility (μ_e) from 1000 to 1600 cm^2 V^{-1} s^{-1}. The relationship between n_e and μ_e of the samples was reported previously,[16] and is summarized in Table I.

We performed high-resolution x-ray diffraction and reciprocal space mapping using a Philips high-resolution diffractometer with Cu $K\alpha_1$ radiation. No tetragonal metal In phase was detected. All of the InN films had a hexagonal structure and their c axes were perpendicular to the sapphire (0001) planes. The lattice constants of InN were determined by using four nonsymmetric reflections with large diffraction angles, and we obtained averages of 3.53(2) Å for the a axis and 5.70(4) Å for the c axis. The orientation of InN$[1\bar{2}10]$ was parallel to $Al_2O_3[10\bar{1}0]$.

Samples were cut into 4 mm squares with their edges parallel to $[10\bar{1}0]$ and $[1\bar{2}10]$. The resistance of the samples was measured by a dc four-probe method with small indium electrodes on the corners of the squares. At present, it is not known how to fabricate the Hall bar without damaging the surface of InN where the surface electron accumulation layer might exist. Therefore, we used the van der Pauw method for the evaluation of the magnetoresistance. The samples were cooled to 0.5 K in a ^{3}He cryostat. The magnetoresistance was measured as functions of field B and the angle θ between the direction of B and the crystal c axis. For the observation of the anisotropic magnetoresistance, a rotating sample holder was used in a 15 T superconducting solenoid. The accuracy of the angle was ±2°. For these measurements, the rotation axis was set along $[10\bar{1}0]$. Hence transverse magnetoresistance (TMR) was obtained when the current was along $[10\bar{1}0]$. When the current was along $[1\bar{2}10]$, TMR was observed when $B\|c$ axis and longitudinal magnetoresistance (LMR) was observed when $B\perp c$ axis.

These samples showed clear photoluminescence and Raman spectra. The carrier density dependence of the luminescence position was expressed well by the Burstein-Moss shift where the band-gap energy of InN was 0.64 eV.[16] In the Fourier transform infrared reflectivity spectra, clear plasma oscillation was observed, and from its energy, the electron effective mass of InN for the nondoped InN was assigned to be $0.085m_0$.[8] The Raman spectra of these samples were clear and sharp, which indicates that Si doping did not degrade the crystal structure. The observed A_1(LO) phonon revealed that there was an electronic continuum in InN even in the samples with the lowest carrier density.

III. RESULTS

A. Temperature dependence of the resistivity

All of the samples investigated showed metallic conductivity, that is, when the temperature decreased, the resistivity (ρ) decreased above 20 K. Typical temperature dependences of ρ for nondoped and Si-doped InN are shown in Fig. 1. The ordinate scale is normalized by the values at 150 K. Above 20 K, ρ does not depend linearly on T but rather on $\sim\sqrt{T}$ and reaches a minimum around 20 K. Below 20 K, ρ increases with the decreasing temperature, which indicates a localization mechanism in the temperature dependence of the resistivity.

In the nondoped InN (no. 252), ρ continues to change smoothly down to 0.5 K without showing any saturation. The temperature dependence of ρ is given by $\rho\sim\log(1/T)$, as is expected from the two-dimensional localization, and not

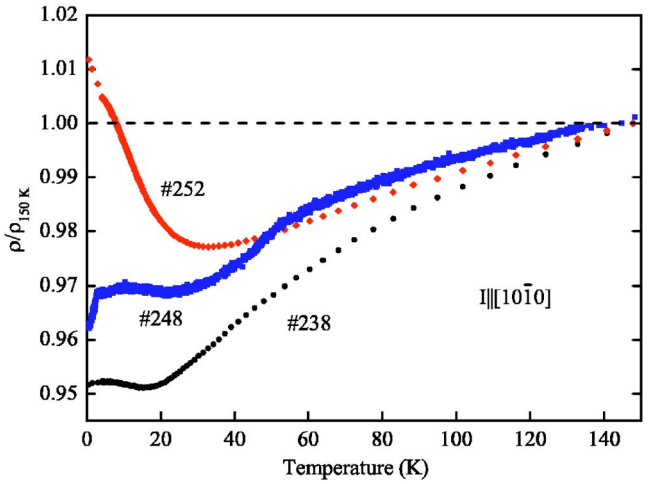

FIG. 1. (Color online) Temperature dependence of the resistivity of typical InN. The ordinate scale is normalized by the values at 150 K. $n_e(10^{18}$ cm$^{-3})$ of no. 252, no. 238, and no. 248 is 1.8, 3.0, and 15, respectively.

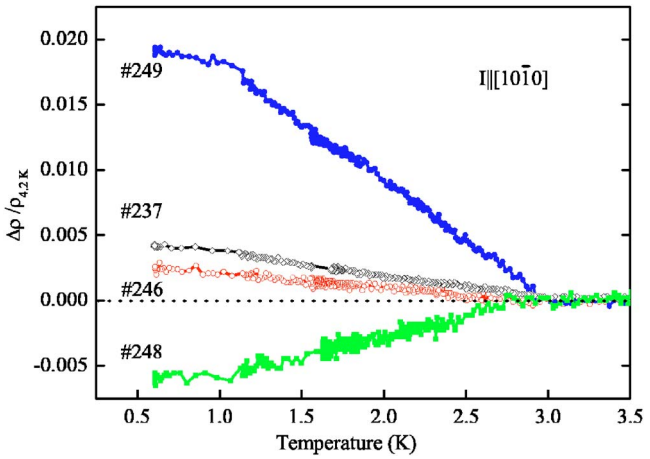

FIG. 2. (Color online) Temperature dependence of the resistivity change $\Delta\rho$ of typical Si-doped InN below 3.5 K. Each value is normalized by the resistivity at 4.2 K. $n_e(10^{18}\ \mathrm{cm}^{-3})$ of no. 237, no. 246, no. 248, and no. 249 is 2.5, 4.7, 15, and 7.0, respectively.

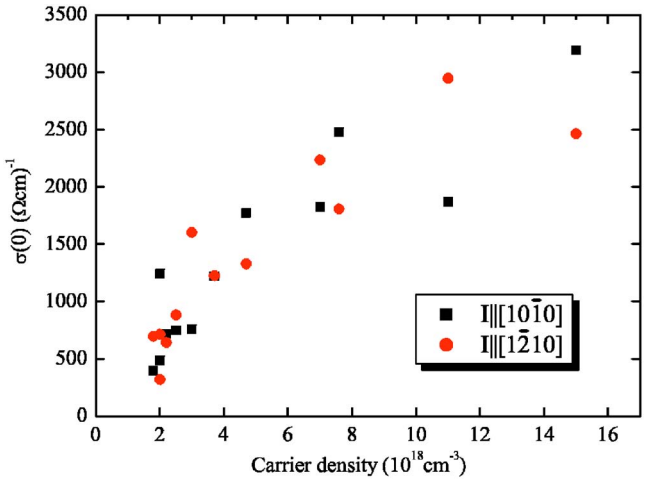

FIG. 3. (Color online) Zero-temperature conductivity $\sigma(0)$ vs carrier density for Si-doped InN. The conductivity depends on the current direction in the a-b plane, and $\sigma(0)$'s are measured for both along $[10\bar{1}0]$ and along $[1\bar{2}10]$.

by $\rho \sim \exp(T_0/T)^{1/4}$, as is expected from the variable-range-hopping conduction mechanism.

When InN is doped with Si, the change of ρ against T is essentially the same as that of the nondoped InN above 20 K, taking a minimum around 20 K. Below 20 K, however, the temperature dependence of ρ is more complex. Typical resistivity changes ($\Delta\rho$) are shown in Fig. 2, where $\Delta\rho$ is normalized by the value at 4.2 K. In samples no. 237 and no. 249, $\Delta\rho$ starts to increase at 3.0 K and in no. 246 at 2.5 K. As for the most heavily doped sample (no. 248), the measured signals are noisy and $\Delta\rho$ starts to decrease at 3 K. The magnitude of the resistivity change is of the order of 10^{-2}, which indicates that the resistivity anomaly originates in the electron localization.

Next we determine the n_e dependence of zero-T conductivity $\sigma(0)$. For our measurements, since the lowest temperature is 0.5 K, we determine $\sigma(0)$ by the value at 0.5 K, though ρ is still changing there. The n_e dependence of $\sigma(0)$ is plotted in Fig. 3. At 0.5 K, $\sigma(0)$ depends on the current direction in the a-b plane of the InN surface, and we plot $\sigma(0)$'s for the current directions of $[10\bar{1}0]$ and $[1\bar{2}10]$, where the geometric correction for the four-probe measurement is set to be 4.53.[17] From the figure, we understand that the investigated InN is a degenerate semiconductor and it is in the metallic side of the Mott transition, and the nondoped InN is very close to the transition.

B. Magnetoresistance

To make clear the weak localization effect in InN, we measured the magnetoresistance $(\Delta\rho/\rho_0=[\rho(B)-\rho(0)]/\rho(0))$ at 0.5 K in two configurations: transverse magnetororesistance (TMR) and longitudinal magnetoresistance (LMR).

A typical TMR of low carrier density with the current I parallel to $[10\bar{1}0]$ is shown in Fig. 4. The applied magnetic field (B) was rotated from parallel ($\theta=0°$) to perpendicular ($\theta=90°$) to the crystal c axis. The TMR shows a monotonic behavior with a relatively small B region. The monotonic part normalized to ρ_0 is proportional to B^2 when $\Delta\rho/\rho_0 \approx 0$ and changes into a linear dependence in the high-field region. There is a negative magnetoresistance (NMR) in the low B region and in the small θ region. In the high-field region, a sinusoidal variation of resistance due to Shubnikov–de Haas (SdH) oscillations is observed. The details of the θ dependence of the NMR are shown in the inset of Fig. 4, where we plot the deviation of the NMR as a function of θ. The deviation is normalized by the difference of resistivity between $\theta=0°$, where a maximum NMR is seen, and $\theta=90°$, where no NMR is seen, when $B=1.9$ T. The solid line shows a cos θ function fitted to the variation. The cos θ dependence of the variation indicates that the NMR exists only in the a-b plane. Moreover, when we sub-

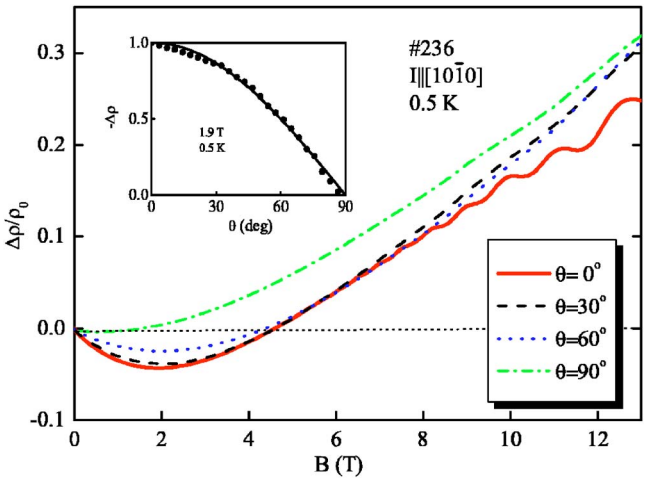

FIG. 4. (Color online) Transverse magnetoresistance of no. 236 ($n_e=2.2\times10^{18}\ \mathrm{cm}^{-3}$) under $I\|[10\bar{1}0]$. The magnetic field is rotated from parallel ($\theta=0°$) to perpendicular ($\theta=90°$) to c axis. Inset shows a variation of the negative magnetoresistance observed at 1.9 T. Solid line is the fitting using a cosine function.

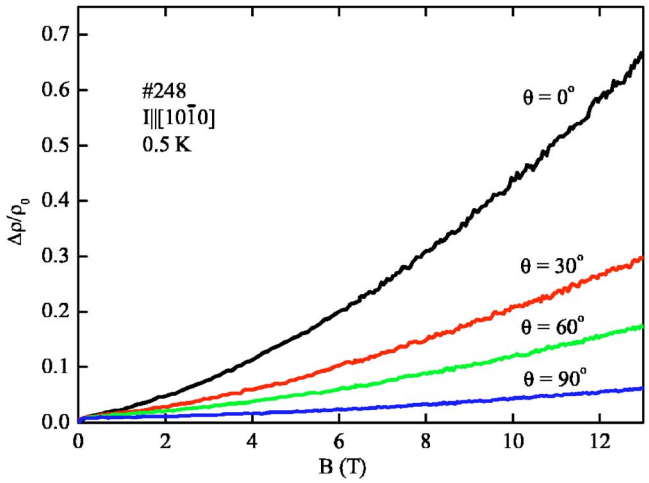

FIG. 5. (Color online) Angle θ dependence of the transverse magnetoresistance of no. 248 ($n_e = 1.5 \times 10^{19}$ cm^{-3}) under $I \| [10\bar{1}0]$.

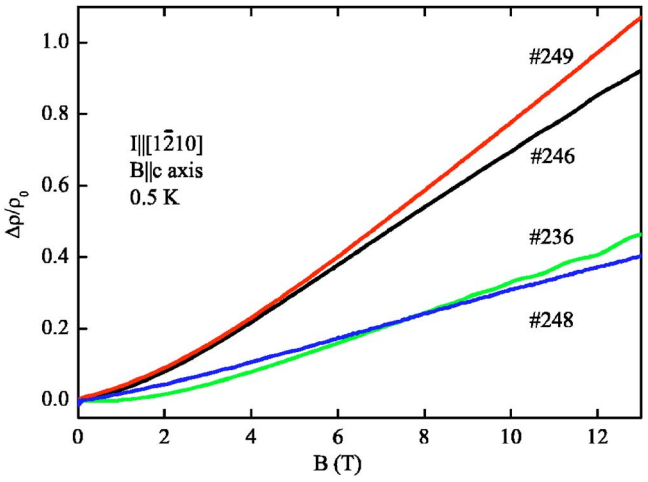

FIG. 6. (Color online) Typical transverse magnetoresistance when $I \| [1\bar{2}10]$ and $B \| c$ axis at 0.5 K. $n_e(10^{18}$ cm$^{-3})$ of no. 236, no. 246, no. 249, and no. 248 is 2.2, 4.7, 7.0, and 15, respectively.

tract the contribution of NMR from the TMR, the θ dependence of the TMR almost disappears.

As for the SdH oscillations observed when $B > 6$ T, oscillations with high frequency exist within several degrees from $\theta = 0°$. Details of the θ dependence were reported previously using sample no. 237.[14] The oscillation frequency changes drastically when $\theta > 5°$. The NMR is obvious at the carrier density lower than 5×10^{18} cm^{-3}, and so is the SdH oscillation.

When the carrier density is higher, only positive TMR is observed under this configuration. Simultaneously, TMR becomes θ-dependent, and the case of the most heavily Si-doped sample is shown in Fig. 5. When $B \| c$ axis, the TMR shows a B^2 dependence up to 13 T without saturation. The θ dependence of TMR is stronger than the cos θ or cos^2 θ dependence.

When the current is along $[1\bar{2}10]$ and $B \| c$ axis, we observe TMR different from those shown in Figs. 4 and 5, which reveals that the conduction mechanism along $[1\bar{2}10]$ is different from that along $[10\bar{1}0]$. Typical TMRs are shown in Fig. 6. In this current direction, no. 236 does not show any NMR in the low B region and its TMR depends linearly on B with SdH oscillations overlapping it in the high B region. The TMR of no. 248 depends linearly on B. Sample no. 246 has the highest n_e of 4.7×10^{18} cm^{-3} among the samples which show SdH oscillations.

In Fig. 7, we show the n_e dependence of LMR. When n_e is smaller than 5×10^{18} cm^{-3}, the LMR has a B^2 dependence with a negative coefficient, and the SdH oscillation overlaps it above 6 T. When n_e increases, a weak NMR is observed in the low B region, but the LMR turns positive above 12 T with the B^2 dependence having a positive slope (no. 247). In no. 250, NMR is no longer observed and only a positive LMR is observed.

In Fig. 8, we summarize the n_e dependences of the TMRs and the LMR at 13 T. As is seen in (a), (c), and (d), $\Delta\rho/\rho_0$ is scattered in the small n_e region owing to the SdH oscillations and the NMR in the a-b plane. There is a change of conduction mechanism around $n_e \simeq 5 \times 10^{18}$ cm^{-3}. When n_e exceeds this density, the NMR disappears and TMR has anisotropy. The $\Delta\rho/\rho_0$ of (b) takes a minimum around $n_e = 2.5 \times 10^{18}$ cm^{-3} and turns from negative to positive around $n_e \simeq 5 \times 10^{18}$ cm^{-3}. Simultaneously, a clear change of $\Delta\rho/\rho_0$ is seen in (a).

C. Shubnikov–de Haas measurements

The SdH oscillation is observed when at least the following two conditions are satisfied. (i) Cyclotron resonance is observed when $\omega_c \tau = \mu_e B \gg 1$. Hence the sample mobility should be much larger than 1000 cm^2 V^{-1} s^{-1}. (ii) Electrons move on the surface of the Fermi sphere, where the cyclotron radius ($\lambda_{cy} = \hbar k_F / eB$) is larger than $\sim 10^{-8}$ m. Hence the grain size of InN should be larger than λ_{cy}. In our experiments, both of the conditions are satisfied at $B > 10$ T.

The movement of Bloch electrons under a strong magnetic field is fixed on the Fermi surface which is cut perpen-

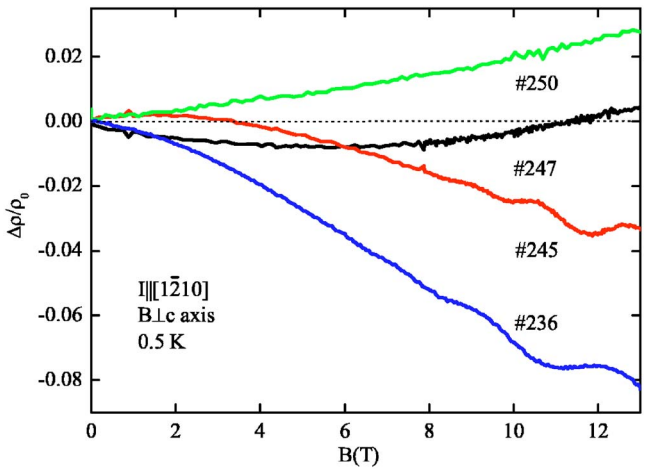

FIG. 7. (Color online) Magnetic-field dependence of longitudinal magnetoresistance for typical samples. $n_e(10^{18}$ cm$^{-3})$ of no. 236, no. 245, no. 247, and no. 250 is 2.2, 3.7, 7.6, and 11, respectively.

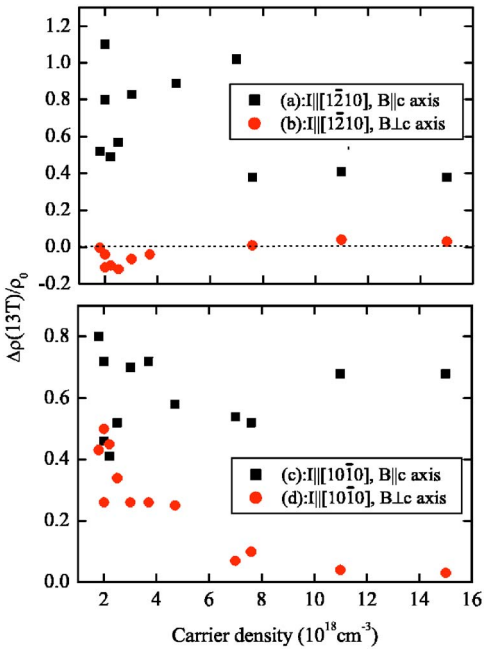

FIG. 8. (Color online) Summary of the carrier density dependence of the magnetoresistance under four configurations. $\Delta\rho(13\ \mathrm{T})/\rho_0$ is the resistivity change at 13 T normalized at 0 T under the configurations indicated.

dicular to field B. When the Fermi sphere is quantized under a strong magnetic field, an oscillatory component ($\Delta\rho$) of the resistivity becomes observable, which is expressed as follows:[18]

$$\Delta\rho(B) \propto \sqrt{\frac{\hbar\omega_c}{2\zeta_n}}\cos\left(\frac{\pi}{2}\frac{gm_e}{m_0}\right)\frac{2\pi^2 k_B T/\hbar\omega_c}{\sinh(2\pi^2 k_B T/\hbar\omega_c)} \times\exp\left(-\frac{2\pi^2 k_B T_D}{\hbar\omega_c}\right)\cos\left(\frac{2\pi\zeta_n}{\hbar\omega_c}-\frac{\pi}{4}\right), \qquad (1)$$

where $\omega_c = eB/m_e$ is the cyclotron frequency, $\zeta_n = \hbar^2 k_F^2/2m_e$ is the Fermi energy, g is the Landé g factor, $T_D = \hbar/(\pi k_B \tau_c)$ is the Dingle temperature, and τ_c is the lifetime of carriers at the Landau level. The phase $\pi/4$ in the last cos term is a variable parameter.

We derived SdH oscillations from the magnetoresistance by fitting the monotonic part as a cubic function of B. The SdH parts of Fig. 4 are shown in Fig. 9. When $B\|c$ axis, the SdH oscillation is large and its frequency is high. At other angles, the amplitude is small and the frequency is low. The SdH oscillation with high frequency can be observed $\theta \leqslant 5°$, the details of which were reported previously.[14]

The SdH oscillation of sample no. 236 in other configurations given in Figs. 6 and 7 is shown in Fig. 10. The SdH amplitude when $B\|c$ axis and $I\|[1\bar{2}10]$ is about half of that obtained when $I\|[10\bar{1}0]$, but the SdH frequency does not change. The SdH oscillation of LMR is similar to that observed at larger angles shown in Fig. 9.

As is seen in Fig. 9, the SdH oscillation at 0° is not a pure-sinusoidal function but it is overlapped by an oscillation at higher angles. To evaluate the mixing ratio of these two

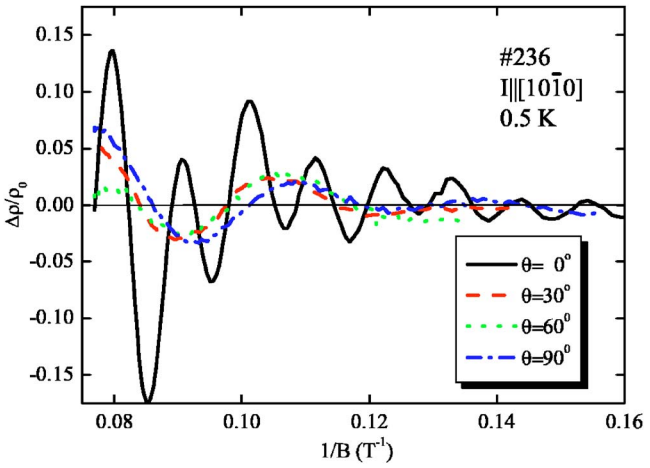

FIG. 9. (Color online) Angle dependence of the SdH oscillations derived from Fig. 4 under $I\|[10\bar{1}0]$ at 0.5 K.

oscillations, the SdH oscillation at 0° is reproduced in Fig. 11 using Eq. (1). At the first step of the fitting, we reproduced the oscillation at 90°, and the initial phase was determined to be $\pi/8$ using $m_e = 0.085m_0$ obtained from the optical measurement.[8] We obtain a Fermi radius $k_{F\perp}$ of $3.22 \times 10^8\ \mathrm{m}^{-1}$ and $T_D = 20$ K, which gives $\tau_c = 1.2 \times 10^{-13}$ s, which is in good agreement with the value obtained from the Hall measurement at 0.5 K, where $\mu_e = 1200\ \mathrm{cm}^2\ \mathrm{V}^{-1}\ \mathrm{s}^{-1}$ and $n_e = 3.5 \times 10^{18}\ \mathrm{cm}^{-3}$. The SdH oscillation at 0° was reproduced using these parameters. When the angle decreases, the initial phase increases and reaches $5\pi/8$ at 0°, whereas $k_{F\perp}$ and its amplitude remain constant. At 0° the oscillation with the Fermi radius of $k_{F\|} = 5.32 \times 10^8\ \mathrm{m}^{-1}$ is overlapped by the oscillation with $k_{F\perp}$, where the former amplitude is five times larger than that of the latter. The values of T_D and m_e are the same for two configurations.

Figure 9 shows that $k_{F\|}$ is observed only around 0°. At other angles, and under the longitudinal configuration, SdH oscillations with $k_{F\perp}$ are observed, suggesting that the Fermi surface or electron effective mass of InN consists of two components: one is spherical with a radius $k_{F\perp}$ and the other is observed in the a-b plane with a radius $k_{F\|}$.

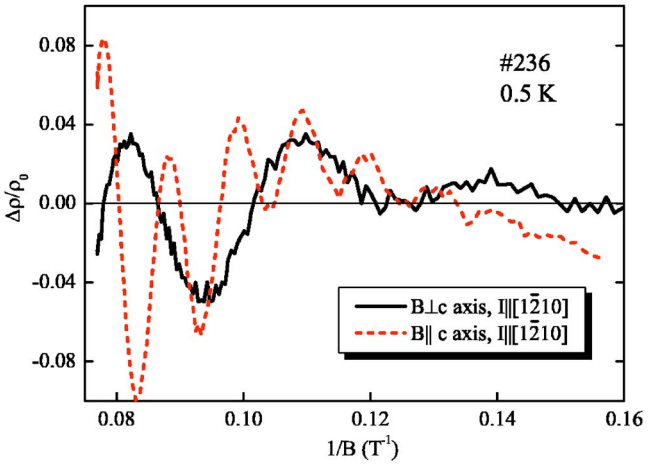

FIG. 10. (Color online) The SdH oscillations of sample no. 236 derived from Figs. 6 and 7.

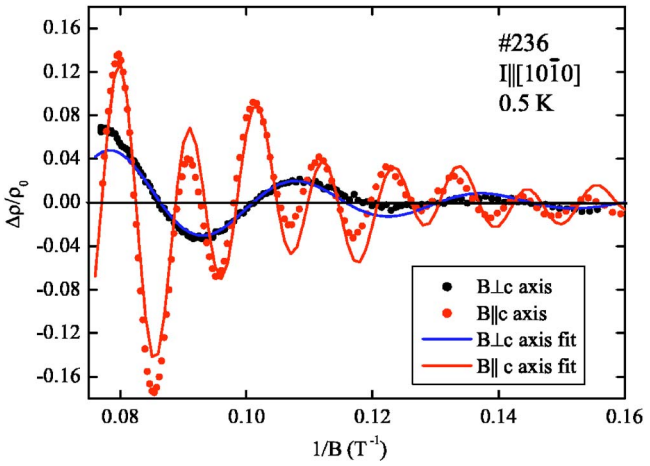

FIG. 11. (Color online) Fitting results of the SdH oscillations shown in Fig. 9. The fittings were done using Eq. (1) for two configurations of $B \| c$ axis and $B \perp c$ axis.

When InN has a spherical Fermi surface, the electron density $N_\perp$ is obtained by

$$N_\perp = (3\pi^2)^{-1} k_{F\perp}^3. \tag{2}$$

Using Eq. (1), we determine n_e dependences of $k_{F\perp}$ and $k_{F\|}$ of the samples which show SdH oscillations. We obtain $N_\perp = 1.1 \times 10^{18}$ cm^{-3} for the sample shown in Fig. 9. The remaining carriers of $N_\| = 1.1 \times 10^{18}$ cm^{-3} belong to the structure observed in the a-b plane. In Fig. 12, we plot $N_\perp$ against n_e obtained by the Hall measurements at room temperatures. The carrier density $N_\|$ with $k_{F\|}$ is not easy to calculate because of its anomalous angle dependence. Hence in the figure, the carrier density $N_\|$ is obtained by subtracting $N_\perp$ from n_e. As is seen in Fig. 12, $N_\perp$ increases linearly against the increase of n_e, but $N_\|$ remains constant, which is consistent with the fact that $k_{F\|}$ does not show n_e dependence. On the average, $k_{F\|}$ is 5.3×10^8 m^{-1}, and the carrier density of 4.5×10^{12} cm^{-2} remains in the a-b plane constantly.

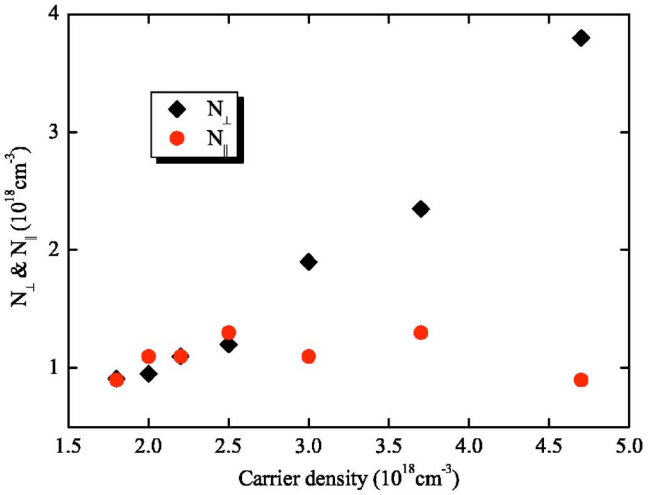

FIG. 12. (Color online) Carrier density (n_e) dependence of $N_\perp$ which is determined by the SdH oscillation. $N_\|$ is obtained by subtracting $N_\perp$ from n_e.

IV. DISCUSSION

A. Critical carrier density for the Mott transition

The n_e dependence of the conductivity in Fig. 3 shows that Si-doped InN is in the metallic side of the metal-insulator transition. The metal-insulator transition of heavily doped semiconductors was investigated in the 1970s and was understood on the basis of Anderson's localization.[19] According to this mechanism, the temperature dependence of the resistivity remains below 1 K, and there is a negative magnetoresistance in the weak-field region.[20] These features are explained by the conducting electrons scattered inelastically by randomly distributed potentials. The reversal of the electron wave vector is due to the constructive interference of electron waves after many elastic scattering events which do not destroy the coherence of the electron waves. In a magnetic field, the constructive interference is prevented and the resistivity is reduced, and then negative magnetoresistance occurs. These features are shown in Figs. 1 and 4.

In the Anderson model, a finite minimum metallic conductivity $\sigma_{\min}$ at zero temperature in a three-dimensional random system is given as follows:[21]

$$\sigma_{\min} \simeq \frac{e^2}{3\pi^2 \hbar a_0}, \tag{3}$$

where a_0 is the lattice constant of InN. When we use $a_0 = 3.53$ Å, $\sigma_{\min} = 240\ (\Omega\ \text{cm})^{-1}$.

Now we estimate n_c of InN, the critical carrier density that causes a metal-insulator transition. According to the scaling theory of localization, we can fit $\sigma(0)$ with the equation[22]

$$\sigma(0) = \sigma_{\min}[(n/n_c) - 1]^\zeta, \tag{4}$$

where $\sigma_{\min} = 240\ (\Omega\ \text{cm})^{-1}$ and ζ is the critical exponent of the localization. As is seen in Fig. 12, there is a constant carrier distribution of 1.0×10^{18} cm^{-3} in the a-b plane as an average, hence we subtract 1.0×10^{18} cm^{-3} from n_e to obtain a substantial carrier density n. Moreover, as $\sigma(0)$ shown in Fig. 3 includes the contribution of $N_\|$, we subtract $270(\Omega\ \text{cm})^{-1}$, which is the conductivity corresponding to 1.0×10^{18} cm^{-3} in the averaged $\sigma(0)$ of nondoped InN. In Fig. 13, we plot corrected $\sigma(0)$ versus n together with the best-fitting curve of Eq. (4) with $n_c = 2 \times 10^{17}$ cm^{-3} and $\zeta = 0.58$. According to the scaling theory, $\zeta = 0.58$ is the case where the Si-doped InN is a noncompensated semiconductor like P-doped Si.[22] At present, it is not clear whether Si impurity is a donor or acceptor in InN, but the experimental results show that n_e increases with the increasing Si-doping concentration and the luminescence peaks shift in accordance with the Moss-Burstein equation.[16] Therefore, it can be said that Si-doped InN is an uncompensated semiconductor in a metallic phase except for the constant carrier density in the a-b plane.

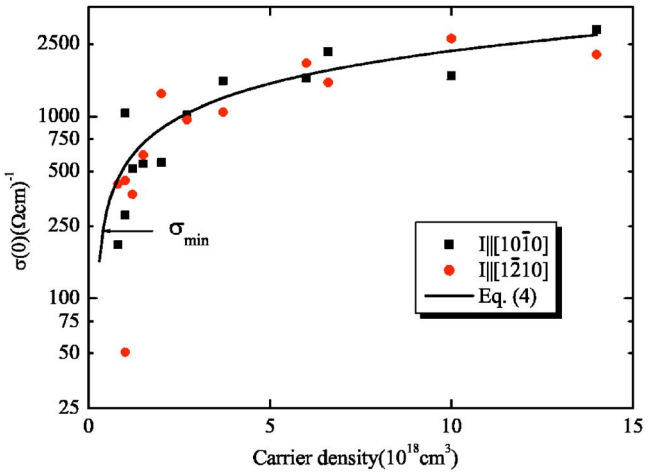

FIG. 13. (Color online) Substantial carrier density dependence of the corrected zero-temperature conductivity $\sigma(0)$. Conductivity $\sigma_{\min}$ is also indicated. The solid line is drawn using Eq. (4), where $\zeta=0.58$, $n_c=2\times10^{17}$ cm^{-3}, and $\sigma_{\min}=240$ $(\Omega$ cm$)^{-1}$.

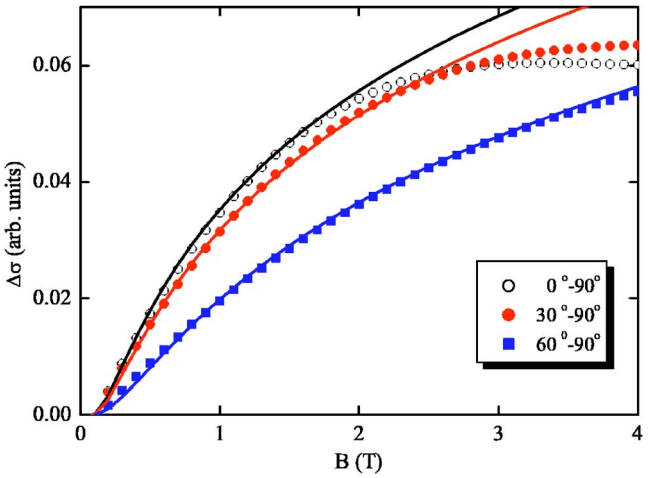

FIG. 14. (Color online) Change in conductivity $\Delta\sigma$ vs magnetic field given in Fig. 4. Solid lines are fitted lines using Eq. (5), where $\tau=8\times10^{-14}$ s, $D=3.2\times10^{-1}$ cm^2 s^{-1}, and $\tau_\epsilon=8\times10^{-11}$ s.

B. Anisotropy of electron localization

We have seen in the previous sections that when the current is along [10$\bar{1}$0], there is NMR, but along [1$\bar{2}$10], it is scarcely observed. As for the SdH oscillation, when the current is along [10$\bar{1}$0] it is clear and strong, whereas along [1$\bar{2}$10] it is not. Therefore, we conclude that there is a nonuniform electronic structure in the a-b plane, though InN belongs to the hexagonal system and the two resistivity tensors normal to the c axis are the same.

According to the theory based on Anderson's localization, and if the component of the electron motion along B is neglected because the NMR shown in Fig. 4 exists only in the a-b plane, the change of conductivity with B applied perpendicular to the surface of heavily doped semiconductors is written as follows:[23]

$$\Delta\sigma(B) = -\frac{\alpha e^2}{2\pi^2\hbar}\left[\psi\left(\frac{1}{2}+\frac{1}{a\tau}\right)-\psi\left(\frac{1}{2}+\frac{1}{a\tau_\epsilon}\right)-\ln\frac{\tau_\epsilon}{\tau}\right], \tag{5}$$

where $a=4DeB/\hbar$, α is a constant prefactor, ψ is a di-gamma function, D is the diffusion coefficient, τ is the relaxation time due to the normal impurity scattering, and τ_ϵ is the inelastic-scattering time of electrons (see Fig. 14). The experimental points are well reproduced by Eq. (5), where $\Delta\rho$ is converted into $\Delta\sigma$. The angle dependence of the field is given by $B\cos\theta$. Using $\tau=8\times10^{-14}$ s, we obtain $D=3.2\times10^{-1}$ cm^2 s^{-1} and $\tau_\epsilon=8\times10^{-11}$ s from the fitting. Value D is close to what is estimated from Einstein's relation given by $D=k_BT\mu_e/e$ [k_B is the Boltzmann constant, $\mu_e=1200$ cm^2 (V s)$^{-1}$, and $D=0.051$ cm^2 s^{-1} at 0.5 K]. Our samples have a film thickness of 250 nm. The diffusion length of the inelastic electron is given by $L_\epsilon=\sqrt{D\tau_\epsilon}$, and hence $L_\epsilon=5.1\times10^{-8}$ m, which is much smaller than the film thickness. This means the anisotropy of the NMR is not caused by the film thickness, but it should be explained by the inelastic scattering of the electrons that move along [10$\bar{1}$0].

Next we consider the anisotropy of the Fermi surface. As is seen in Fig. 9, the Fermi surface of InN consists of two components: one is spherical with $k_{F\perp}$ and the other is observed in the a-b plane with $k_{F\parallel}$. One of the possible explanations for the SdH oscillation in the a-b plane is that it is caused by the accumulation layer at the surface or at the interface of heteroepitaxy. Recently, Lu *et al.* reported on the surface charge accumulation of InN observed by C-V measurements[24] using samples with $n_e\simeq2\times10^{18}$ cm^{-3}, and Mahboob *et al.* confirmed this finding by high-resolution electron-energy-loss spectroscopy measurements.[25] Their sheet charge was of the order of 2.5×10^{13} cm^{-2}, which is one order of magnitude larger than what we observed. Swartz *et al.* reported, by the variable magnetic-field Hall measurement, that the mobility of the surface electron, though in their analysis the low mobility electron was labeled as a surface electron based on the prior C-V measurements, was much smaller than that of the bulk and was less than 1000 cm^2 V^{-1} s^{-1}.[26] If it is so, $\omega_c\tau<1$, and we cannot observe SdH oscillations originating from the electrons accumulated at the surface. There is a possibility that our sample has an electron layer with the mobility high enough to satisfy $\omega_c\tau>1$, because the sheet charge density of our samples is 4.5×10^{12} cm^{-2}. In this case, we can expect that the oscillations depend only on the perpendicular component of the field, and the period follows $(B\cos\theta)^{-1}$ as is observed in a semiconductor superlattice with two-dimensional (2D) electron distribution.[27] For example, some passivated n-type mercury-cadmium-telluride photoconductive infrared detectors have 2D electron accumulation layers ($n_e\sim10^{12}$ cm^{-2}) at the surfaces, whose SdH peak varies as $(\cos\theta)^{-1}$.[28] However, the angle dependence of SdH signals shown in Fig. 9 is not expressed by $(\cos\theta)^{-1}$ dependence. Besides, the SdH oscillation in our experiments depends on the current direction and n_e. Therefore, we conclude that the SdH oscillation with $k_{F\parallel}$ does not come from the electrons accumulated at the surface, even if an electron accumulation layer exists.

One of the characteristics of the SdH oscillation of InN is that it is amplified as the NMR becomes stronger when $B \| c$ axis. Considering that the NMR is due to the constructive coherence of the electron waves in the *a-b* plane, the SdH oscillation with $k_{F\|}$ should have been caused by the electron waves spread in the plane, which forms special Fermi surfaces that contribute quantum oscillations to the TMR and LMR. The Fermi surface, as the simplest form, has the shape of a flat ellipsoid with the shortest diameter along the normal to the *a-b* plane.

Regarding nondoped InN as being very close to the Mott transition, we can expect strong correlation effects in the temperature dependence of the resistivity. In the case of a heavily doped semiconductor, it is written as follows:

$$\rho(T) = \rho_0 + \rho_{\mathrm{ph}}(T) + \rho_{\mathrm{cor}}(T). \quad (6)$$

In this equation, ρ_0 is the term due to the impurity or defect scattering and has no temperature dependence. The second term comes from the phonon scattering and is expressed by the Grüneisen term, which has a negligible contribution below 4.2 K. The third term originates from the localization due to the electron-electron correlation and has a very weak contribution. The experimental results shown in Figs. 1 and 2 however, are indicative of the importance of the last term of this equation. Such an anomalous temperature dependence of resistivity has been reported for heavily doped semiconductors like Ge:Sb and was explained in the framework of *s-d* interaction.[29] We suppose that a similar mechanism exists in InN because InN is expected to have a strong spin-orbit interaction originating in the *d*-electron mixing at the top of the valence band.[30] The contribution of the last term is positive or negative according to the inelastic-scattering mechanism.[31] For example, when the coherence of the electron waves is dominant in the inelastic scattering, it is positive. When the spin-orbit coupling is dominant, it is negative. As is seen in Figs. 1 and 2, nondoped InN shows a log T dependence, and when Si is doped, the coefficient becomes positive or negative. These features are evidence to show that the term ρ_{cor}(T) is dominant along $[10\bar{1}0]$ below 3 K.

The presence of surface and interface layers would significantly affect the zero-field resistivity. Since surface accumulation layers are not electrically insulated from the bulk, resistivity measurements of degenerate semiconductors can be difficult. This difficulty is removed if the bulk carriers can be frozen onto the impurities or the subbands by using low temperature and by applying a high magnetic field. At present, there has been no report of subbands at the surface electron accumulation layer of InN, and this subject needs further investigation.

The difference between $[10\bar{1}0]$ and $[1\bar{2}10]$ is the atom arrangement in the *a-b* plane. When the current is along $[10\bar{1}0]$, electrons move with the atom spacing of 6.12 Å, and along $[1\bar{2}10]$, they move with the atom spacing of 3.54 Å, which is the length of the *a* axis. Thus at low temperatures, the conduction electrons are sensitive to the difference of the distance. The angular dependence of the NMR in Fig. 5 suggests that the NMR does not originate in a spin mechanism but it is an effect of the orbital motion of the electrons in the *a-b* plane. Moreover, the fact that the NMR has a weak temperature dependence between 0.5 and 4.2 K indicates that the localization is not sensitive to the change of temperature.

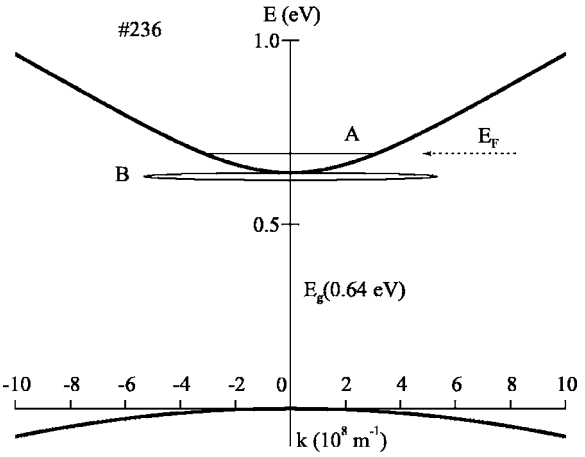

FIG. 15. Electronic structure of sample no. 236 illustrated assuming the band-gap energy of 0.64 eV. The free-electron effective mass was calculated assuming a nonparabolic (E_p=10 eV) dispersion. The hole effective mass of $m_h=0.5m_0$ is tentative. There is a spherical Fermi surface denoted by *A*. There is an additional structure of a flat ellipsoid denoted by *B*, which has the largest diameter in the *a-b* plane. The effective mass of *B* is anisotropic and is much larger than that of *A*.

The most possible mechanism that will account for the anisotropy of NMR and the anomalous SdH oscillation in the *a-b* plane is the contribution of the core *d* electrons of In atoms. As was mentioned before, the core *d* electrons play essential roles in the band structure and the lattice-dynamics calculations. Moreover, a strong *s-d* coupling has been reported for InN.[32] In this case, the wave functions of *d* electrons are mixed with the conduction band of InN and cause the anisotropy of the localization in the *a-b* plane. Consequently, the effective mass of the conduction electrons in the *a-b* plane becomes heavier than that in the other directions, which produces a structure in the spherical Fermi surface of InN.

C. Band structure of InN at the fundamental absorption edge

The band structure of InN has been discussed mainly on the basis of calculations that were performed to agree with the data by optical measurements.[33] The obtained band structures were similar to those of other III-nitride compounds. The magnetoresistance results, however, suggest that the band structure of InN is more complex. Based on the magnetoresistance results, we illustrate the band structure of sample no. 236 in Fig. 15. For the drawing, we use the band-gap energy of 0.64 eV assuming a nonparabolic dispersion for the conduction band so as to meet the n_e dependence of the photomuninescence spectra, where an energy parameter related to the momentum matrix element (E_p) is 10 eV.[16]

From the SdH oscillation, sample no. 236 has a spherical Fermi surface with the radius $k_{F\perp}=3.2\times10^8$ m^{-1}, which is denoted by *A*. The structure observed when the field is per-

pendicular to the *a*-*b* plane is drawn as a flat ellipsoid with the largest radius $k_{F\|}=5.3\times10^{8}$ m^{-1}, which is denoted by *B*. The effective mass of *B* is anisotropic and is much larger than that of *A*. The energy position of the latter should be lower than that of the former because $k_{F\perp}$ increases according to the increase of n_e while $k_{F\|}$ does not. This suggests *B* has a limited volume and is fully occupied, and that the carriers introduced into no. 236 lift the Fermi level of *A*. The structure is connected to the Fermi surface and the electrons belonging to *B* can migrate into the *a*-*b* plane.

The band structure given in Fig. 15 explains the drastic change of the TMR at $n_e\simeq5\times10^{18}$ cm^{-3}. When the carrier density increases, $k_{F\perp}$ increases and exceeds $k_{F\|}=5.3\times10^{8}$ m^{-1} at $n_e\simeq5\times10^{18}$ cm^{-3} from Eq. (2). When n_e exceeds this carrier density, the NMR and the SdH oscillation observed in the *a*-*b* plane disappear and the θ dependence of TMR becomes obvious. Simultaneously, the LMR shown in Fig. 7 increases quadratically against *B*. When the Fermi surface is spherical like *A*, that is, when the effective mass, relaxation time, and mobility are scalar quantities, there is no LMR. When there is nonvanishing LMR, there should be a special electronic structure.[34] These features indicate that there is a drastic change of the electronic structure of InN at $n_e\simeq5\times10^{18}$ cm^{-3}.

The change of the band structure was observed in the n_e dependence of the photoluminescence spectra, where the peak position deviated from the Moss-Burstein shift at $n_e\simeq5\times10^{18}$ cm^{-3}.[16] Wu *et al.* reported two types of temperature dependence of the luminescence.[35] When $n_e=3.5\times10^{17}$ cm^{-3}, the luminescence peak shifts with the temperature change according to the band-gap energy, and when $n_e=1.2\times10^{19}$ cm^{-3}, the luminescence peak does not depend on temperature and is observed 150 meV below the band-gap energy. This result is another piece of evidence to show that there is an electronic-structure change between these two n_e's. In a previous paper, we reported that the Raman spectra of Si-doped InN revealed that the A_1(LO) phonon and free carriers couple nonlinearly and Fano interferences are prominent between the zone-center LO phonon and the quasicontinuum electronic state,[8] which is consistent with the results presented here.

V. CONCLUSION

We have investigated the temperature dependence of the resistivity of InN as a function of carrier density. The investigated InN belongs to heavily doped semiconductors in the metallic side of the Mott transition and the critical carrier density of the Mott transition was estimated to be 2×10^{17} cm^{-3}. There was a resistivity anomaly originating in the carrier localization in the *a*-*b* plane, and also there was a localization anisotropy between $[10\bar{1}0]$ and $[1\bar{2}10]$. The *d* electrons of In atoms are considered to be the cause of the anisotropy in the *a*-*b* plane. The Shubnikov–de Haas oscillation shows that InN has a spherical Fermi surface and its radius increases according to the increase of the carrier density when $n_e<5\times10^{18}$ cm^{-3}. There is an additional structure observed when the field is perpendicular to the *a*-*b* plane. The structure is considered to be due to the contribution of the *d* electrons, which causes the effective mass of the conduction electrons in the *a*-*b* plane to be heavier than those in other directions. The structure has a constant carrier density of 4.5×10^{12} cm^{-2} in the *a*-*b* plane. The carrier density dependence of the magnetoresistance reveals that the electronic structure changes around $n_e\sim5\times10^{18}$ cm^{-3}.

ACKNOWLEDGMENTS

The authors are grateful to Professor T. Yao of Tohoku University for his help, to the Ministry of Education, Science, Sports, and Culture of Japan for the Grant-in-Aid for Scientific Research No. 17560293, and to the Nippon Sheet Glass Foundation for the financial suport. The low-temperature measurement was carried out at the High Field Laboratory for Superconducting Materials of Tohoku University.

*Email address: inushima@keyaki.cc.u-tokai.ac.jp

[1] S. Nakamura and F. Fasol, *Blue Laser Diode* (Springer-Verlag, Berlin, 1997).
[2] T. Inushima, V. V. Mamutin, V. A. Vekshin, S. V. Ivanov, T. Sakon, S. Motokawa, and S. Ohoya, J. Cryst. Growth **227–228**, 481 (2001).
[3] T. Inushima, V. V. Mamutin, V. A. Vekshin, S. V. Ivanov, V. V. Davydov, T. Sakon, and M. Motokawa, Phys. Status Solidi B **228**, 9 (2001).
[4] T. Inushima, T. Takenobu, M. Motokawa, K. Koide, A. Hashimoto, A. Yamamoto, Y. Saito, T. Yamaguchi, and Y. Nanishi, Phys. Status Solidi C **0**, 364 (2002).
[5] V. Y. Davydov, *et al.*, Phys. Status Solidi B **229**, R1 (2002).
[6] J. Wu, W. Walukiewicz, K. M. Yu, J. W. Ager III, E. E. Haller, H. Lu, W. J. Schaff, Y. Saito, and Y. Nanishi, Appl. Phys. Lett. **80**, 3967 (2002).
[7] T. Matsuoka, H. Okamoto, M. Nakao, H. Harima, and E. Kurimoto, Appl. Phys. Lett. **81**, 1246 (2002).
[8] T. Inushima, M. Higashiwaki, and T. Matsui, Phys. Rev. B **68**, 235204 (2003).
[9] S. Wei, X. Nie, I. G. Batyrev, and S. B. Zhang, Phys. Rev. B **67**, 165209 (2003).
[10] T. Inushima, T. Shiraishi, and V. Y. Davydov, Solid State Commun. **110**, 491 (1999).
[11] V. Y. Davydov, V. V. Emtsuev, I. N. Goncharuk, A. N. Smirnov, V. D. Petrikov, V. V. Mamutin, V. A. Vekshin, S. V. Ivanov, M. B. Smirnov, and T. Inushima, Appl. Phys. Lett. **75**, 3297 (1999).
[12] C. Bungaro, K. Rapcewicz, and J. Bernholc, Phys. Rev. B **61**, 6720 (2000).
[13] J. Wu, W. Walukiewicz, K. M. Yu, J. W. Ager III, E. E. Haller, H. Lu, W. J. Schaff, Y. Saito, and Y. Nanishi, Appl. Phys. Lett. **80**, 4741 (2002).
[14] T. Inushima, M. Higashiwaki, T. Matsui, T. Takenobu, and M. Motokawa, Phys. Status Solidi C **0**, 2822 (2003).

[15] M. Higashiwaki and T. Matsui, Jpn. J. Appl. Phys., Part 2 **41**, L540 (2002).
[16] M. Higashiwaki, T. Inushima, and T. Matsui, Phys. Status Solidi B **240**, 417 (2003).
[17] L. J. van der Pauw, Philips Tech. Rev. **20**, 220 (1958).
[18] K. Seeger, *Semiconductor Physics*, 5th ed., Solid-State Sciences Vol. 40 (Springer-Verlag, Berlin, 1991).
[19] P. W. Anderson, Phys. Rev. **109**, 1492 (1958).
[20] Y. Ootuka and A. Kawabata, Prog. Theor. Phys. Suppl. **84**, 249 (1985).
[21] B. I. Shklovkii and A. L. Efros, *Electronic Properties of Doped Semiconductors*, Solid-State Sciences Vol. 45 (Springer-Verlag, Berlin, 1984).
[22] T. F. Rosenbaum, K. Andres, G. A. Thomas, and R. N. Bhatt, Phys. Rev. Lett. **45**, 1723 (1980).
[23] S. Kawaji and T. Kawaguchi, in *Application of High Magnetic Fields in Semiconductor Physics*, *Lecture Notes in Physics 177*, edited by G. Landwehr (Springer Verlag, Berlin, 1983), p. 53.
[24] H. Lu, W. J. Schaff, L. F. Eastman, and C. E. Stutz, Appl. Phys. Lett. **82**, 3254 (2003).
[25] I. Mahboob, T. D. Veal, C. F. McConville, H. Lu, and W. J. Schaff, Phys. Rev. Lett. **92**, 036804 (2004).
[26] C. H. Swartz, R. P. Tompkins, N. C. Giles, T. H. Myers, H. Lu, W. J. Schaff, and L. F. Eastman, J. Cryst. Growth **269**, 29 (2004).
[27] L. L. Chang, H. Sakaki, C. A. Chang, and L. Esaki, Phys. Rev. Lett. **38**, 1489 (1977).
[28] J. R. Lowney, D. G. Seiler, W. R. Thurber, Z. Yu, X. N. Song, and C. L. Littler, J. Electron. Mater. **22**, 985 (1993).
[29] Y. Ootuka, S. Kobayashi, S. Ikehata, W. Sasaki, and J. Kondo, Solid State Commun. **30**, 169 (1979).
[30] M. Cardona and N. E. Christensen, Solid State Commun. **116**, 421 (2000).
[31] Y. Nagaoka, Prog. Theor. Phys. Suppl. **84**, 1 (1985).
[32] C. Persson and A. Zunger, Phys. Rev. B **68**, 073205 (2003).
[33] F. Bechstedt and J. Furthmüller, J. Cryst. Growth **246**, 315 (2002).
[34] E. Fawcett, Adv. Phys. **13**, 139 (1964).
[35] J. Wu, W. Walukiewicz, W. Shan, K. M. Yu, S. X. L. J. W. Ager III, E. E. Haller, H. Lu, and W. Schaff, J. Appl. Phys. **94**, 4457 (2003).